Flame monitoring of a model swirl injector 1D tunable diode laser absorption spectroscopy tomography

Flame monitoring of a model swirl injector using 1D tunable diode laser absorption spectroscopy tomography

2017 Meas. Sci. Technol. 28 054002

(http://iopscience.iop.org/0957-0233/28/5/054002)

IOP Publishing Measurement Science and Technology
Meas. Sci. Technol. **28** (2017) 054002 (8pp) https://doi.org/10.1088/1361-6501/aa5aee

Flame monitoring of a model swirl injector using 1D tunable diode laser absorption spectroscopy tomography

Chang Liu[1,2,3], Zhang Cao[1,2], Fangyan Li[1,2], Yuzhen Lin[4] and Lijun Xu[1,2]

[1] School of Instrument Science and Opto-Electronic Engineering, Beihang University, Beijing 100191, People's Republic of China
[2] Ministry of Education's Key Laboratory of Precision Opto-mechatronics Technology, Beijing 100191, People's Republic of China
[3] Laboratory for Air Pollution and Environmental Technology, Empa, 8600 Dübendorf, Switzerland
[4] School of Energy and Power Engineering, Beihang University, Beijing 100191, People's Republic of China

E-mail: lijunxu@buaa.edu.cn

Received 4 December 2016, revised 15 January 2017
Accepted for publication 20 January 2017
Published 3 March 2017

Abstract

Distributions of temperature and H_2O concentration in a swirling flame are critical to evaluate the performance of a gas turbine combustor. In this paper, 1D tunable diode laser absorption spectroscopy tomography (1D-TDLAST) was introduced to monitor swirling flames generated from a model swirl injector by simultaneously reconstructing the rotationally symmetric distributions of temperature and H_2O concentration. The optical system was sufficiently simplified by introducing only one fan-beam illumination and a linear detector array of 12 equally-spaced photodetectors. The fan-beam illumination penetrated a cross section of interest in the swirling flame and the transmitted intensities were detected by the detector array. With the transmitted intensities in hand, projections were extracted and employed by a 1D tomographic algorithm to reconstruct the distributions of temperature and H_2O concentration. The route of the precessing vortex core generated in the swirling flame can be easily inferred from the reconstructed profiles of temperature and H_2O concentration at different heights above the nozzle of the swirl injector.

Keywords: swirling flame, swirl injector, tunable diode laser absorption spectroscopy (TDLAS), 1D tomography, temperature, species concentration

(Some figures may appear in colour only in the online journal)

1. Introduction

Flame stability is one of the most critical factors in evaluating the combustion efficiency, pollutant emissions and lifetime of a gas turbine combustor. In recent years, lean-premixed (LPM) combustion technology has been widely used because of the increasingly strict regulations for pollutant emissions [1, 2]. As the system usually operates near the lean blowout limit with low equivalent ratio in LPM combustion, a small perturbation in the equivalent ratio may generate a significant variation in heat release and further causes flame oscillations [3]. In practical applications of LPM combustion, swirl injectors are employed extensively in the combustors to generate swirling flows of the reactants and hence swirling flames [4, 5]. The swirling flames enable high energy conversion in a small volume and exhibit good ignition and stabilization behavior over a wide operating range.

The characteristics of the swirling flame mainly include structure, temperature and species concentrations of the flow field [5]. Particularly, the temperature indicates the combustion efficiency and influences the lifetime of the gas turbine, while the species concentrations are most directly related to the pollutant emissions. On one hand, the temperature and species concentrations are very useful, in particular for the combustion

engineers, to optimize the structure of the swirl injectors and thus improve the performance of the gas turbine. On the other hand, they are important parameters for validating the computational models to simulate the swirling flame and further provide reliable references for the numerical calculations in fluid dynamics and thermodynamics. Therefore, it is necessary to develop efficient combustion diagnostic techniques to monitor the temperature and species concentrations of the swirling flame.

As non-intrusive and sensitive optical modalities, laser-based combustion diagnostic techniques are widely used to measure the temperature and species concentrations of the swirling flame. For instance, Thariyan *et al* developed and implemented a dual-pump coherent anti-Stokes Raman scattering (CARS) system to measure temperature and major species concentrations of the swirling flame in the gas turbine combustor [6]. Richardson *et al* reconstructed the distributions of temperature and carbon-monoxide in the atmospheric-pressure inverse diffusion flames using two-color planar laser-induced fluorescence (PLIF) [7]. Stopper *et al* measured the temperature and species of the swirling flames using 1D laser Raman scattering [8]. Kiefer *et al* analyzed the mixing and combustion phenomena in turbulent partially premixed flames using laser-induced breakdown spectroscopy (LIBS) [9]. Williams *et al* applied laser-induced thermal gratings spectroscopy (LITGS) to measure the temperature in a firing gasoline direct injection engine [10]. Although these attempts are effective to measure the temperature and species concentrations of the swirling flame, the experimental systems require complicated optics, high-power laser sources and clean operating environment, which are often hard to meet.

Tunable diode laser absorption spectroscopy (TDLAS) is a robust, sensitive, fast response and low cost technique for measuring temperature and species concentrations in the flow field [11–17]. Given that the averaged swirling flame is rotationally symmetric during a period of stable operation, the TDLAS technique can be combined with 1D tomography [18, 19], referred to as 1D-TDLAST hereafter, to retrieve the radial distributions of temperature and species concentrations over the cross sections of interest in the swirling flame.

By employing the 1D-TDLAST technique, the distributions of temperature and H_2O concentration over typical cross sections of interest in the swirling flame generated by a model swirl injector were reconstructed in this paper. The optical system was sufficiently simplified by introducing only one fan-beam illumination and a linear detector array of 12 equally-spaced photodetectors. To validate the proposed method, the results obtained from the 1D-TDLAST technique were compared with the computational fluid dynamics (CFD) simulation results under different combustion conditions.

2. Methodology

According to the previous reports [4, 20], although the instantaneous images over a cross section of the swirling flame may be asymmetric, the image accumulated or averaged from hundreds of instantaneous flame images is symmetric. Given that the structure of the swirl injectors and their nozzles are rotationally symmetric, the averaged distributions of temperature and species concentrations over a cross section of the swirling flame should be rotationally symmetric too. In this way, 1D-TDLAST technique can be applied to reconstruct the rotationally symmetric distributions of temperature and species concentrations over the cross sections of interest in the swirling flame. Firstly, the fundamentals on TDLAS will be briefly reviewed. Then, the 1D-TDLAST technique and system for monitoring the swirling flame will be introduced in this section.

2.1. Fundamentals on TDLAS

When a laser beam at frequency v (cm^{-1}) penetrates a flame with a total path length of L (cm), the transmitted intensity I_t is related to the incident intensity I_0 by

$$\left(\frac{I_t}{I_0}\right)_v = \exp\left(-\int_0^L P(l)X_{abs}(l)S\left[T(l)\right]\phi \mathrm{d}l\right), \quad (1)$$

where $P(l)$ (atm) is the local total pressure, $S[T(l)]$ ($cm^{-2}\,atm^{-1}$) the temperature dependent line strength of the molecular transition of the absorbing species, $X_{abs}(l)$ the local mole fraction of the absorbing species, ϕ the line-shape function [21]. The absorbance α_v is defined as

$$\alpha_v = -\ln\left(\frac{I_t}{I_0}\right)_v = \int_0^L P(l)X_{abs}(l)S\left[T(l)\right]\phi \mathrm{d}l. \quad (2)$$

Because the line-shape function ϕ is normalized, so that $\int_{-\infty}^{\infty}\phi \mathrm{d}v \equiv 1$, the integrated absorbance A of the molecular transition can be inferred from equation (2) as

$$A = \int_{-\infty}^{+\infty}\alpha_v \mathrm{d}v = \int_0^L P(l)X_{abs}(l)S\left[T(l)\right]\ \mathrm{d}l. \quad (3)$$

2.2. 1D TDLAST

Figure 1 depicts the schematic diagram of a 1D-TDLAST system. The system mainly includes two distributed feedback (DFB) laser diodes at different transitions (v_1 and v_2), two DFB laser control modules, a 1D-TDLAST sensor, a data acquisition card and a computer. The linewidth and maximum output power of the DFB laser diodes are 2 MHz and 20 mW, respectively. Each of the DFB laser diodes is independently controlled with a DFB laser control module by adjusting temperature and injection current. The two DFB laser diodes work with a time division multiplexing scheme [22, 23]. To be specific, each laser diode is driven by a ramp signal at a repetition rate of 10 kHz, while the phase difference between the driven signals of the two DFB laser diodes is 180°. That is to say, during a scanning period, only one DFB laser diode is driven to output laser, while the other is stopped by setting the injection current under the lower working threshold.

The outputs of the two DFB laser diodes are combined with a single-mode fiber coupler, and split into two channels.

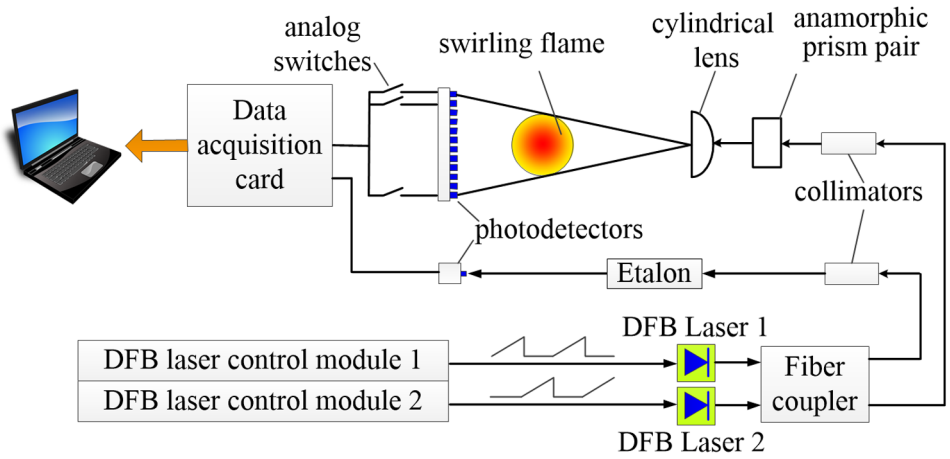

Figure 1. Schematic diagram of the 1D-TDLAST system.

The laser in the first channel penetrates through an etalon to monitor the frequency during the wavelength scanning process. The laser in the second channel is collimated first and penetrates through an anamorphic prism pair and a cylindrical lens to form a fan-beam illumination. As noted in our previous works [24, 25], the implementation of the anamorphic prism pair is effective to improve the uniformity of the fan-shaped planar illumination, and hence improving the fidelity of image reconstruction. Then, the fan-beam illumination penetrates the cross section of interest in the swirling flame and is detected by the linear array of 12 equally-spaced photodetectors. In conjunction with the analog switches, the transmitted intensities are obtained by the photodetectors independently and sampled by the data acquisition card. The sampled data are finally used to calculate the integrated absorbance areas, i.e. the projections. Justified by the smooth variation of temperature and H_2O concentration, the 12 projections are interpolated into a total number of 31 projections using spline interpolation to obtain a smoother display in a higher number of grids. Finally, the interpolated projections for 100 repetitive measurements are averaged. The averaged projections, noted as A, are used in the 1D-TDLAST technique to reconstruct the radial distributions of temperature and H_2O concentration over the cross section of interest in the swirling flame. It should be noted that the left-hand side and right-hand side averaged projections from the center of the fan-beam illumination display mirrored as the flame is rotationally symmetric. The right-hand side projections were used in the experiment to reconstruct the radial distributions of temperature and H_2O concentration. The redundant left-hand side projections were used to justify the rotationally symmetric assumption of the swirling flame, which will be detailed in section 3.

An absorption hygrometer was used to obtain the ambient humidity. As shown in figure 2(a), Given the arrangements of the fan-beam laser paths, the integrated absorbance area of the i-th laser beam for the laser path outside the region of interest, i.e. $A_{\mathrm{air},i}$, can be calculated by

$$A_{\mathrm{air},i} = PS(T_{\mathrm{air}})X_{\mathrm{air}}L_{\mathrm{air},i}, \tag{4}$$

where the pressure P equals 1 atm, T_{air} equals 300 K, X_{air} is the measured ambient humidity. $L_{\mathrm{air},i}$ is the path length out of the region of interest for the i-th laser beam. Therefore, the projection for the ith laser beam, i.e. A_i, can be calculated by subtracting $A_{\mathrm{air},i}$ from the measured integrated absorbance $A_{\mathrm{meas},i}$.

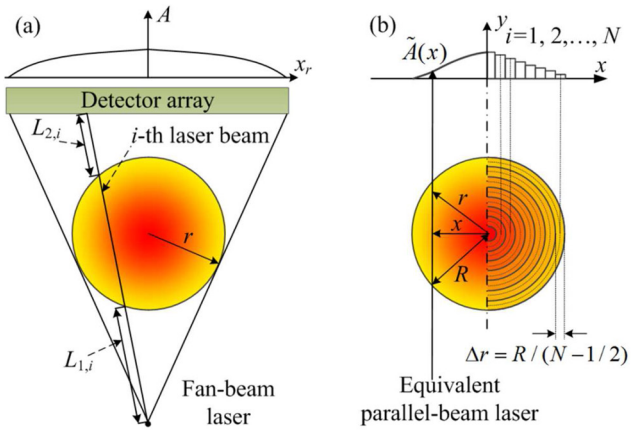

Figure 2. Illustration of (a) fan-beam geometry and (b) equivalent parallel-beam geometry for a rotationally symmetric swirling flame.

To simplify the optical system, the fan-beam illumination was used in this work instead of the parallel-beam illumination, as shown in figure 2(a). Given that the averaged swirling flame is rotationally symmetric, Abel equations can be used to retrieve the radial distributions of temperature and H_2O concentration. It should be noted that Abel equations are established for parallel-beam projections. Therefore, the fan-beam geometry should be firstly transformed into equivalent parallel-beam geometry with appropriate interpolations, as detailed in [26]. We suppose the averaged A in the fan-beam geometry be corresponding to $\tilde{A}(x)$ in the parallel-beam geometry.

In the equivalent parallel-beam geometry, the origin of the coordinate system is at the center of the swirling flame with radius R. The cross section of the flame is discretized into N equal-spaced concentric circles, as shown in figure 2(b). The interval of two adjacent concentric circles Δr equals to $R/(N - 1/2)$. The radius of the i-th concentric circle is $r_i = i\Delta r$, $i = 1, \ldots, N$. As the averaged swirling flame is rotationally symmetric, the pressure, temperature and H_2O concentration

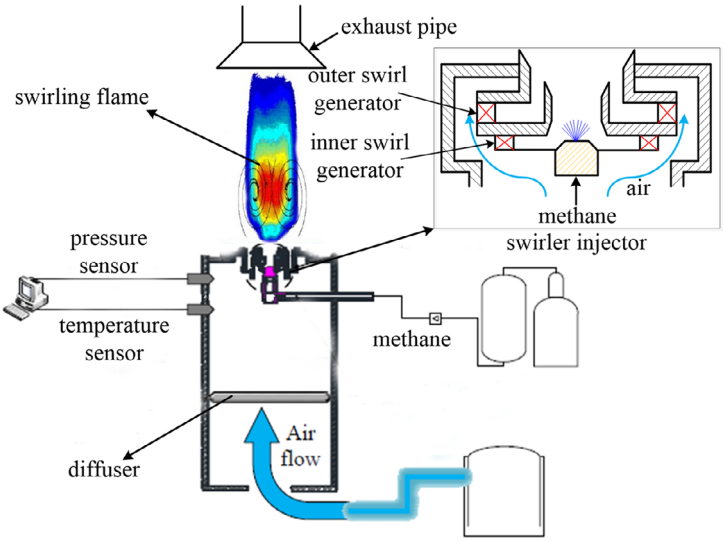

Figure 3. Schematic diagram of the experimental platform for swirl combustion.

in the i-th circle are uniform, noted as $P(r_i)$, $T(r_i)$ and $X(r_i)$, respectively. The density of the integrated absorbance $a(r_i)$ can be expressed as

$$a(r_i) = P(r_i) \cdot S\,[T(r_i)] \cdot X(r_i). \tag{5}$$

N equivalent parallel laser beams, with interval Δr, penetrate the cross section of the swirling flame along y-axis. The coordinate of the intersection of the ith laser beam and x-axis is $x_i = i\Delta r$. Therefore, the relationship between $\tilde{A}(x_i)$ and $a(r_i)$ can be described by the Abel's integral equation as follows:

$$\widetilde{A}(x_i) = 2\sum_{j=i}^{N} \int_{\substack{r_i, j=i \\ r_j-\Delta r/2, j>i}}^{r_j+\Delta r/2} \frac{a(r_j)\tilde{r}}{\sqrt{\tilde{r}^2 - x_i^2}} \mathrm{d}\tilde{r}, \tag{6}$$

Through Abel inversion, $a(r_i)$ can be solved by

$$a(r_i) = -\frac{1}{\pi} \int_{\substack{r_i, j=i \\ r_j-\Delta r/2, j>i}}^{r_j+\Delta r/2} \frac{\widetilde{A}'(x_j+\delta)}{\sqrt{(x_j+\delta)^2 - r_i^2}} \mathrm{d}\delta, \tag{7}$$

where $A(x_i)$ is approximated into a quadratic form in the neighbor of x_i, noted as the three-point Abel deconvolution [18], i.e.

$$A'(x_i+\delta) = \frac{A(x_{i+1}) - A(x_{i-1})}{2\Delta r} + \frac{A(x_{i+1}) + A(x_{i-1}) - A(x_i)}{\Delta r^2} \cdot \delta. \tag{8}$$

By using the two-color absorption spectroscopy strategy, the radial distribution of temperature $T(r_i)$ can then be retrieved from equation (5), as

$$T(r_i) = \frac{\frac{hc}{k}(E_2'' - E_1'')}{\ln \frac{a_1(r_i)}{a_2(r_i)} + \ln \frac{S_2(T_0)}{S_1(T_0)} + \frac{hc}{k}\frac{(E_2'' - E_1'')}{T_0}}. \tag{9}$$

With $T(r_i)$ in hand, the distribution of H_2O concentration $X(r_i)$ can be calculated at an atmospheric pressure by:

$$X(r_i) = \frac{a_1(r_i)}{S_1\,[T(r_i)]}. \tag{10}$$

3. Experiments and results

3.1. Experimental setup

In the experiment, the swirling flame was generated on an experimental platform for swirl combustion. As shown in figure 3, the experimental platform includes air and methane supply systems, a plenum chamber with temperature and pressure sensors, a model swirl injector and an exhaust pipe with a conical top plate. In detail, the air supply system contains an air tank, a pressure-release valve and an orifice meter for air flow measurement, while the methane supply system contains a methane tank, a pressure-release valve and a mass flowmeter for methane flow measurement. In the experiment, the dry air at room temperature entered the plenum chamber and went through a diffuser. After the diffuser, the uniformly distributed dry air flowed through two swirl generators, named as inner and outer swirl generators, respectively. The non-swirling methane was fed through the central nozzle and mixed with the swirled air from the inner swirl generator. Then, the mixed fuel and air was further mixed with the swirled air from the outer swirl generator. To increase the shearing force of the flow, the inner and outer swirl generators swirled clockwise and anti-clockwise, respectively. In this way, the mixing extent of air and methane was significantly improved, which contributed to higher combustion efficiency. After ignition, an unconfined swirling flame was generated above the nozzle of the swirl injector. The diameter of the nozzle was 42 mm. The feedbacks obtained from the temperature and pressure sensors were used to control the pressure-release valve of the air supply system in real time and maintain a stable working condition in the plenum chamber. Finally, unburnt methane exited the exhaust pipe for safety.

Figure 4 depicts the 3D sketch of the 1D-TDLAST sensor that was mounted on the experimental platform. As a major product of the combustion of hydrocarbons, H_2O was selected as the target absorbing species. The central frequencies of the two DFB laser diodes were selected at 7444.36 cm^{-1}

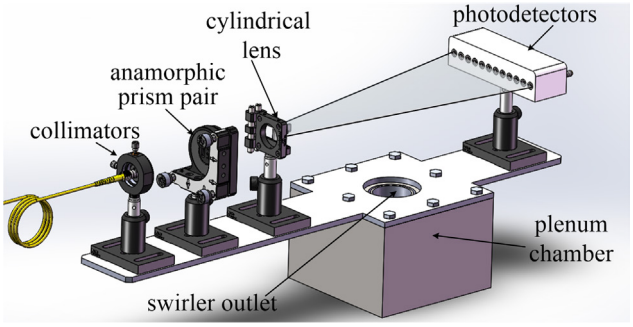

Figure 4. 3D sketch of the 1D-TDLAST sensor.

and 7185.6 cm^{-1}, because of the moderate line strengths and good temperature sensitivity of H_2O transitions at these two frequencies [22, 23, 25, 27, 28]. The laser was first collimated using the collimator (CFC-5X-C, Thorlabs). Then, the well collimated laser with the diameter of the laser spot about 0.5 mm was guided through the anamorphic prism pair (PS-883-C, Thorlabs) and the cylindrical lens (LJ1918L2-C, Thorlabs). In this way, the fan-beam illumination with a span angle of 24° was generated. The fan-beam illumination completely covered the cross section of interest in the swirling flame and was finally detected by the linear detector array of 12 equally-spaced photodetectors. The height of the fan-beam illumination can be adjusted to obtain the flame profiles at different heights above the nozzle of the model swirl injector.

3.2. Experimental results

In case of LPM combustion, the flows of methane and air are critical to the flame profile and flame stability. In practical experiments, the flows of methane and air should be precisely controlled to generate the swirling flame. To provide references for the experimental operations, the swirling flames were first simulated using CFD by the aid of ANSYS FLUENT. In addition, the distributions of temperature and H_2O concentration of the swirling flame obtained from the CFD simulation were compared with those reconstructed using the 1D-TDLAST technique.

In the simulation, a 3D computation domain for the flow field of the swirling flame was established. The model of the swirl injector was of the same structure and size of that used in the experiment, as shown in figure 5. The computation domain was discretized using the semiautomatic meshing tool. The air and methane inlets were set as the velocity inlets, while the outlet of the cylindrical combustion volume was set as the pressure outlet. The solver was defined as a 3D pressure-based steady solver. The viscous model was specified as a standard k-epsilon model for turbulent applications. The combustion model was defined using a probability density function table. Since heat transfer in the system was considered here, the energy equations were involved in the simulation.

Given the flows of methane and air, the average distributions of temperature and H_2O concentration were obtained after the iterative calculation was converged. Figure 6 shows the simulation results when the flows of methane and air were

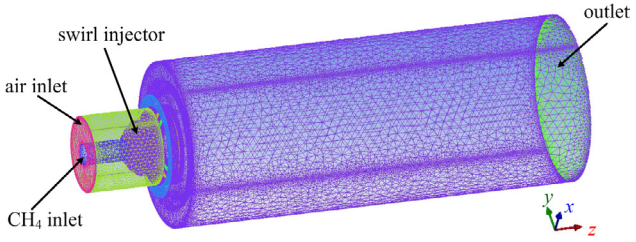

Figure 5. 3D computation domain of the flow field of the swirling flame.

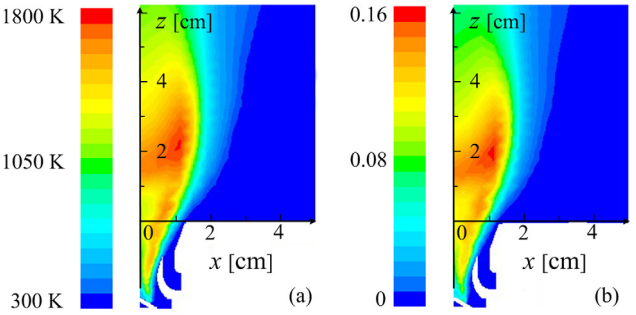

Figure 6. CFD simulation results of the swirling flame with methane and air flows being set as 8 and 371 l min^{-1}, respectively. (a) and (b) Show the contours of temperature and H_2O concentration in the plane x–o–z of the computation domain, respectively.

sets as 8 and 371 l min^{-1}, respectively. With the above settings, a swirling flame under the condition of LPM combustion was generated. The contours of temperature and H_2O concentration in the plane x–o–z of the computation domain are shown in figures 6(a) and (b), respectively. As the swirling flame is rotationally symmetric, the simulation results on the positive x-axis side are only shown for simplicity.

The height above the nozzle of the swirl injector is noted as z. The radial distributions of temperature, ${}^{S}T$, and H_2O concentration, ${}^{S}X$, were extracted from figure 6 at the height of 2 and 4 cm above the nozzle, i.e. $z = 2$ cm and $z = 4$ cm, as shown in figure 7. The experiments were carried out with the same flows of methane and air. To validate the proposed method, the fan-beam illumination was also mounted both at $z = 2$ cm and $z = 4$ cm, respectively. The radial distributions of temperature, ${}^{R}T$, and H_2O concentration, ${}^{R}X$, were reconstructed from 50 repetitive experiments. Each midpoint in the curves denotes the mean of 50 solutions of either ${}^{R}T$ or ${}^{R}X$, while the error bar to each midpoint denotes the standard deviation of the 50 solutions.

It can be seen that the reconstructed profiles of temperature and H_2O concentration agree well with the CFD simulation results. Over the cross sections of interest in the swirling flame, both the experimental and simulation results show that the temperature and H_2O concentration increase from the flame center to the maximum values along the radius, and then gradually decrease because of the heat transfer between the swirling flame and the surrounding air. The peak values of ${}^{R}T$ and ${}^{R}X$ at $z = 2$ cm locate at $x = 1$ cm, while those at $z = 4$ cm locate at $x = 1.38$ cm. The reconstructed

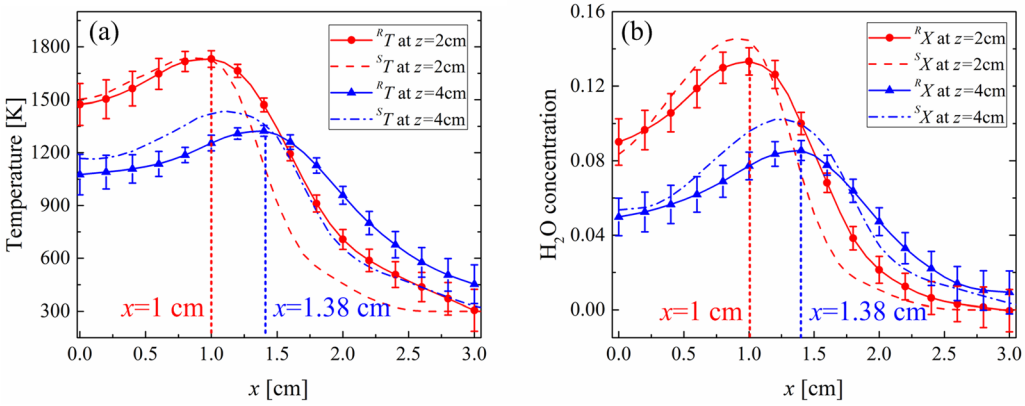

Figure 7. Simulated and experimentally reconstructed distributions of (a) temperature and (b) H_2O concentration at two heights above the nozzle with the flows of methane and air being set as 8 and 371 l min^{-1}, respectively.

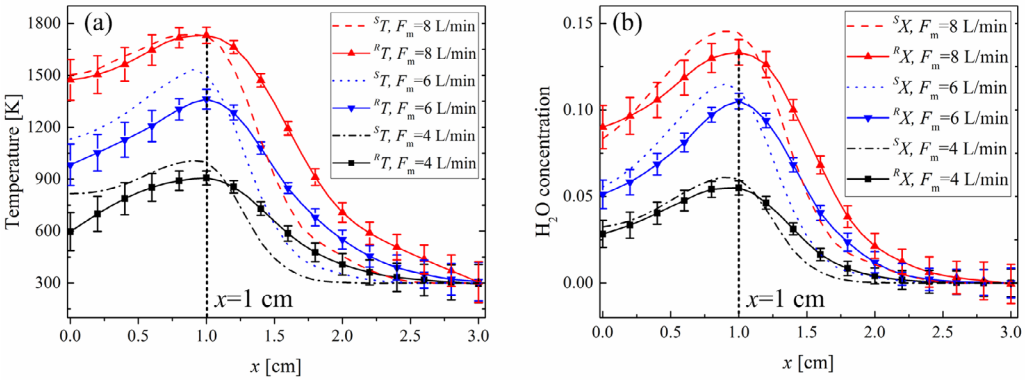

Figure 8. Simulated and experimentally reconstructed distributions of (a) temperature and (b) H_2O concentration at $z = 2$ cm for different equivalent ratios. The air flow was set as 371 l min^{-1}, while the methane flows, noted as F_m, were set as 4, 6 and 8 l min^{-1}, respectively.

temperature and H_2O concentration at $z = 2$ cm are higher than those at $z = 4$ cm from the center to $x = 1.5$ cm, while they are lower than those at $z = 4$ cm from $x = 1.5$ cm towards the flame boundary. The peak of the temperature profile for the flame moves outward in the swirling flame from $z = 2$ cm to $z = 4$ cm. Given that the heat release of the flame is aligned with the precessing vortex core (PVC) located in the swirling flame [20], it can be deduced that the PVC goes upward and gradually deviates from the flame center. In addition, when x is closer to 0, the three-point Abel deconvolution is more ill-posed, which results in larger standard deviations of ^{R}T and ^{R}X. On the boundary of the flame, the weak H_2O absorbance leads to low signal-to-noise ratio. Therefore, the standard deviations of ^{R}T and ^{R}X become larger at the boundary of the flame. It should be noted that the actual spatial resolution of the 1D-TDLAST system mainly depends on the space between each two neighboring photodetectors. In this work, the photodetectors (G12180-010A, Hamamatsu) with a diameter of 0.5 cm were employed in the 1D-TDLAST system, resulting in a space between each two neighboring photodetectors larger than 0.5 cm. In the detector array, the actual space of neighboring photodetectors is 1 cm. Given a detector array with smaller space of neighboring photodetectors, a higher spatial resolution could be achieved.

To study the dependence of the profile of the swirling flame on the equivalent ratio, the air flow was maintained at 371 l min^{-1}, while the methane flow was gradually decreased from 8 l min^{-1} to 4 l min^{-1}. That is to say, the equivalent ratio was reduced and the characteristic of the swirling flame was much closer to the lean blowout limit [20]. Figure 8 shows the simulated and experimentally reconstructed distributions of temperature and H_2O concentration at $z = 2$ cm with different methane flows. The reconstructed profiles of the temperature and H_2O concentration agrees, by and large, with those obtained using the CFD simulation. It can be seen that the temperature and H_2O concentration decrease as the equivalent ratio decreases in both the simulation and experiment results. The peaks of the ^{R}T and ^{R}X locate at around $x = 1$ cm for the three cases with different methane flows.

Furthermore, the 1D-TDLAST technique was employed under the assumption that the averaged distributions of temperature and species concentrations over the cross sections of interest in the swirling flame were rotationally symmetric. Therefore, the left-hand side and right-hand side photodetectors from the center of the fan-beam illumination should display mirrored projection data. In the experiment, 12 equally-spaced photodetectors with serial number $n = 1$, 2,…, 12 were employed to validate the rotational symmetry of

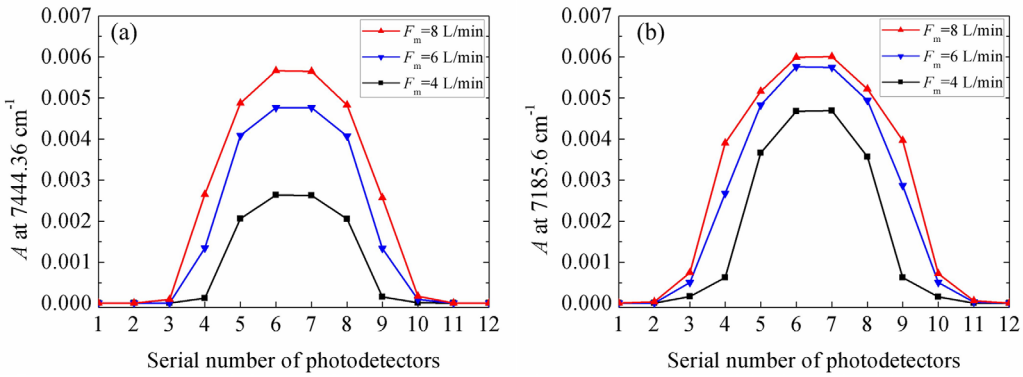

Figure 9. For different equivalent ratios, the averaged integrated absorbance areas obtained by the 12 photodetectors at $z = 2$ cm and at transitions (a) 7444.36 cm^{-1} and (b) 7185.6 cm^{-1}, respectively.

the swirling flame. After mounting the fan-beam illumination, the fan-beam laser source, the center of the cross section of interest in the swirling flame and the midpoint of the detector array located on an identical straight line. The projection data obtained from the photodetectors on the right-hand side ($n = 7, 8, \ldots, 12$) were used to reconstruct the radial distributions of temperature and H_2O concentration. The redundant projections obtained from the other six photodetectors on the left-hand side ($n = 1, 2, \ldots, 6$) were used to justify the rotationally symmetric assumption of the swirling flame.

The experiments were carried out when the air flow was set as 371 l min^{-1}, and the methane flows were set as 4, 6 and 8 l min^{-1}, respectively. At each equivalent ratio, the averaged integrated absorbance areas of 50 repetitive experiments at the transitions 7444.36 cm^{-1} and 7185.6 cm^{-1}, i.e. the projections obtained by the 12 photodetectors were calculated at $z = 2$ cm and shown in figures 9(a) and (b), respectively. For each equivalent ratio, it can be seen that the projections obtained by the photodetectors on the left-hand side can be mirrored to those on the right-hand side. According to equations (5), (6), (9) and (10), the distributions of temperature and H_2O concentration over the cross sections of interest in the swirling flame at each equivalent ratio can be assumed to be rotationally symmetric.

4. Conclusions

The radial distributions of temperature and H_2O concentration over two cross sections of interest in the swirling flame were reconstructed using the 1D-TDLAST technique. In the experiment, the swirling flame was generated using a model swirl injector. The measurement system with a fan-beam illumination and a linear detector array of 12 photodetectors was established to realize the 1D-TDLAST technique. At the same height above the nozzle of the swirl injector, the reconstructed profiles of temperature and H_2O concentration agree well with those obtained from the CFD simulation, denoting that the proposed technique is effective to reconstruct the radial distributions of temperature and H_2O concentration of the swirling flame. With the same combustion condition, the reconstructed profiles of temperature and H_2O concentration at different heights above the nozzle were used to trace the precessing vortex core in the swirling flame. In addition, the radial distributions of temperature and H_2O concentration were reconstructed when the swirling flame was close to the lean blowout limit. The results show that the peaks of the temperature and H_2O concentration profiles located at same radius in the ROI when the air flow was maintained and methane flow was decreased from 8 to 4 l min^{-1}. Furthermore, a detector array with a smaller detector space will contribute to a higher spatial resolution in the reconstructed distributions of the temperature and H_2O concentration. The proposed technique and system in this work provides an effective and low cost way to monitor the swirling flame and analyze the flame characteristics in practical applications.

Acknowledgments

The authors gratefully acknowledge the financial support from the National Science Foundation of China (Grant Nos. 61327011, 613111201 and 61620106004) and the Program for Changjiang Scholars and Innovative Research Team in University (IRT1203).

References

[1] Huang Y and Yang V 2009 Dynamics and stability of lean-premixed swirl-stabilized combustion *Prog. Energy Combust. Sci.* **35** 293–364

[2] Fackler K B, Karalus M, Novosselov I, Kramlich J, Malte P and Vijlee S 2016 NO_x behavior for lean-premixed combustion of alternative gaseous fuels *J. Eng. Gas Turbines Power* **138** 041504

[3] Temme J E, Allison P M and Driscoll J F 2014 Combustion instability of a lean premixed prevaporized gas turbine combustor studied using phase-averaged PIV *Combust. Flame* **161** 958–70

[4] Palies P, Durox D, Schuller T and Candel S 2010 The combined dynamics of swirler and turbulent premixed swirling flames *Combust. Flame* **157** 1698–717

[5] Weigand P, Meier W, Duan X R, Stricker W and Aigner M 2006 Investigations of swirl flames in a gas turbine model combustor: I. Flow field, structures, temperature, and species distributions *Combust. Flame* **144** 205–24

[6] Thariyan M P, Bhuiyan A H, Meyer S E, Naik S V, Gore J P and Lucht R P 2011 Dual-pump coherent anti-Stokes Raman scattering system for temperature and species measurements in an optically accessible high-pressure gas turbine combustor facility *Meas. Sci. Technol.* **22** 015301

[7] Richardson D R, Jiang N, Blunck D L, Gord J R and Roy S 2016 Characterization of inverse diffusion flames in vitiated cross flows via two-photon planar laser-induced fluorescence of CO and 2D thermometry *Combust. Flame* **168** 270–85
[8] Stopper U, Meier W, Sadanandan R, Stöhr M, Aigner M and Bulat G 2013 Experimental study of industrial gas turbine flames including quantification of pressure influence on flow field, fuel/air premixing and flame shape *Combust. Flame* **160** 2103–18
[9] Kiefer J, Li Z and Alden M 2013 Laser-induced breakdown spectroscopy in a partially premixed turbulent jet flame *Meas. Sci. Technol.* **24** 075205
[10] Williams B, Edwards M, Stone R, Williams J and Ewart P 2014 High precision in-cylinder gas thermometry using laser induced gratings: quantitative measurement of evaporative cooling with gasoline/alcohol blends in a GDI optical engine *Combust. Flame* **161** 270–9
[11] Bolshov M A, Kuritsyn Y A and Romanovskii Y V 2015 Tunable diode laser spectroscopy as a technique for combustion diagnostics *Spectrochim. Acta* B **106** 45–66
[12] Cai W and Kaminski C 2017 Tomographic absorption spectroscopy for the study of gas dynamics and reactive flows *Prog. Energy Combust. Sci.* **59** 1–31
[13] Dreier T and Schulz C 2016 Laser-based diagnostics in the gas-phase synthesis of inorganic nanoparticles *Powder Technol.* **287** 226–38
[14] Liu C, Xu L and Cao Z 2013 Measurement of nonuniform temperature and concentration distributions by combining line-of-sight TDLAS with regularization methods *Appl. Opt.* **52** 4827–42
[15] Zhang G, Liu J, Xu Z, He Y and Kan R 2016 Characterization of temperature non-uniformity over a premixed CH_4 air flame based on line-of-sight TDLAS *Appl. Phys.* B **122** 1–9
[16] Li S, Farooq A and Hanson R K 2011 H_2O temperature sensor for low-pressure flames using tunable diodelaser absorption near 2.9 μm *Meas. Sci. Technol.* **22** 125301
[17] Wang F, Cen K F, Li N, Jeffries J B, Huang Q X, Yan J H and Chi Y 2010 Two-dimensional tomography for gas concentration and temperature distributions based on tunable diode laser absorption spectroscopy *Meas. Sci. Technol.* **21** 045301
[18] Dasch C J 1992 One-dimensional tomography: a comparison of abel, onion-peeling, and filtered backprojection methods *Appl. Opt.* **31** 1146–52
[19] Villarreal R and Varghese P 2005 Frequency-resolved absorption tomography with tunable diode lasers *Appl. Opt.* **44** 6786–95
[20] Stöhr M, Boxx I, Carter C and Meier W 2011 Dynamics of lean blowout of a swirl-stabilized flame in a gas turbine model combustor *Proc. Combust. Inst.* **33** 2953–60
[21] Allen M G 1998 Diode laser absorption sensors for gas-dynamic and combustion flows *Meas. Sci. Technol.* **9** 545–62
[22] Liu C, Xu L, Cao Z and McCann H 2014 Reconstruction of axisymmetric temperature and gas concentration distributions by combining fan-beam TDLAS with onion-peeling deconvolution *IEEE Trans. Instrum. Meas.* **63** 3067–75
[23] Xu L, Liu C, Zheng D, Cao Z and Cai W 2014 Digital signal processor-based high-precision on-line Voigt lineshape fitting for direct absorption spectroscopy *Rev. Sci. Instrum.* **85** 123108
[24] Liu C, Xu L, Chen J, Cao Z, Lin Y and Cai W 2015 Development of a fan-beam TDLAS-based tomographic sensor for rapid imaging of temperature and gas concentration *Opt. Express* **23** 22494–511
[25] Xu L, Liu C, Jing W, Cao Z, Xue X and Lin Y 2016 Tunable diode laser absorption spectroscopy-based tomography system for on-line monitoring of two-dimensional distributions of temperature and H_2O mole fraction *Rev. Sci. Instrum.* **87** 013101
[26] Hsich J 2009 *Computed Tomography Principles, Design, Artifacts, and Recent Advances* (Bellingham, WA: SPIE Press)
[27] Li F, Yu X, Gu H, Li Z, Zhao Y, Ma L, Chen L and Chang X 2011 Simultaneous measurements of multiple flow parameters for scramjet characterization using tunable diode-laser sensors *Appl. Opt.* **50** 6697–707
[28] Liu C, Xu L, Li F, Cao Z, Tsekenis S and McCann H 2015 Resolution-doubled one-dimensional wavelength modulation spectroscopy tomography for flame flatness validation of a flat-flame burner *Appl. Phys.* B **120** 407–16